



# Subcortical Visual Shell Nuclei Targeted by ipRGCs Develop from a Sox14+-GABAergic Progenitor and Require Sox14 to Regulate Daily Activity Rhythms

Alessio Delogu,¹ Katherine Sellers,¹ Laskaro Zagoraiou,⁴,⁶ Alina Bocianowska-Zbrog,² Shyamali Mandal,³ Jordi Guimera,⁵ John L.R. Rubenstein,³ David Sugden,² Thomas Jessell,⁴ and Andrew Lumsden¹,\*

<sup>1</sup>MRC Centre for Developmental Neurobiology

<sup>2</sup>Division of Women's Health

School of Medicine, King's College London, London SE1 1UL, UK

<sup>3</sup>Nina Ireland Laboratory of Developmental Neurobiology, Department of Psychiatry, University of California, San Francisco, San Francisco, CA 94143, USA

<sup>4</sup>Department of Biochemistry and Molecular Biophysics, Howard Hughes Medical Institute, Kavli Institute for Brain Science, Columbia University, New York, NY 10032, USA

<sup>5</sup>Deutsches Forschungszentrum für Gesundheit und Umwelt, Helmholtz Zentrum München, Ingolstädter Landstraße 1, D-85764 Neuherberg, Germany

<sup>6</sup>Present address: Biomedical Research Foundation of the Academy of Athens, 4 Soranou Ephessiou Street, 115 27 Athens, Greece

\*Correspondence: andrew.lumsden@kcl.ac.uk

http://dx.doi.org/10.1016/j.neuron.2012.06.013

### **SUMMARY**

Intrinsically photosensitive retinal ganglion cells (ipRGCs) and their nuclear targets in the subcortical visual shell (SVS) are components of the nonimage-forming visual system, which regulates important physiological processes, including photoentrainment of the circadian rhythm. While ipRGCs have been the subject of much recent research, less is known about their central targets and how they develop to support specific behavioral functions. We describe Sox14 as a marker to follow the ontogeny of the SVS and find that the complex forms from two narrow stripes of Dlx2-negative GABAergic progenitors in the early diencephalon through sequential waves of tangential migration. We characterize the requirement for Sox14 to orchestrate the correct distribution of neurons among the different nuclei of the network and describe how Sox14 expression is required both to ensure robustness in circadian entrainment and for masking of motor activity.

### **INTRODUCTION**

The recent discovery of a new class of retinal photoreceptors, melanopsin-expressing intrinsically photosensitive retinal ganglion cells (ipRGCs), revived interest in the role played by light in regulation of certain animal behaviors. Among the behavioral and physiological responses that rely on ipRGCs are entrainment of the circadian rhythm at the hypothalamic suprachiasmatic nucleus (SCN), the induction of the pupillary light reflex (PLR), and the suppression of motor activity (negative

masking) (Berson et al., 2002; Fu et al., 2005; Güler et al., 2008; Hatori et al., 2008; Hattar et al., 2002; Lucas et al., 2001). IpRGCs project directly to the SCN via the glutamatergic retinohypothalamic tract, a pathway that is thought to be sufficient for photoentrainment. IpRGC collaterals extend further than the SCN to reach other targets in the diencephalon, among them the intergeniculate leaflet (IGL) and the olivary pretectal nucleus (OPN) (Hattar et al., 2002). Several lesion-based experiments have implicated these non-SCN ipRGC targets in entrainment of the circadian rhythm (Edelstein and Amir, 1999; Harrington and Rusak, 1989; Johnson et al., 1989; Morin and Pace, 2002; Dkhissi-Benyahya et al., 2000; Muscat and Morin, 2006) and induction of the PLR (Whiteley et al., 1998; Young and Lund, 1994), while data on their involvement in masking of motor activity by light remain sparse and inconclusive (Edelstein and Amir, 1999; Redlin et al., 1999). Yet, defects in photoentrainment were shown to be rather mild and damage to neighboring regions could not be entirely excluded.

The IGL and the OPN are part of a distributed structure known as the subcortical visual shell (SVS) (Moore et al., 2000; Morin and Blanchard, 1998, 2005), consisting of several reciprocally interconnected GABAergic nuclei that, like the SCN, respond to acute light changes by induction of the immediate early gene *c-fos* (Prichard et al., 2002). Further supporting a functional link among the different components of the SVS, both the IGL and OPN display synchronized oscillatory firing patterns (Szkudlarek et al., 2008).

The significance of the ipRGC collaterals reaching several diencephalic targets other than the SCN remains obscure. The complex architecture and interconnectivity of the SVS suggests that it may not just act as a relay for ipRGC signals but serve as an integrator for multiple environmental stimuli, including luminance. It is yet unclear whether the anatomical complexity of the SVS reflects a similarly complex developmental ontogeny. With the aim of understanding the developmental process of SVS formation and to test for a link between its architecture



and the behaviors it controls, we looked at the establishment of specific neuronal lineages within the diencephalon during embryogenesis and hypothesized that within this pool there would also be progenitors for the SVS. While it is accepted that the SVS is a GABAergic complex, GABAergic neurogenesis in the diencephalon has received much less attention than its telencephalic counterpart. Inhibitory diencephalic neurons were initially thought to arise in the prethalamus (rostral diencephalon) and to colonize the caudal diencephalon via tangential migration (Jones, 2007). More recently, we and others have reported that GABAergic neurogenesis occurs in situ in a narrow transverse stripe of cells in the rostral part of the embryonic thalamus (r-Th) (Kataoka and Shimogori, 2008; Scholpp et al., 2009; Vue et al., 2007). GABAergic progenitors in the r-Th can be distinguished from those in the prethalamus by expression of Tal1 (Scholpp et al., 2009), a bHLH transcription factor required for survival of GABAergic progenitors in different regions of the central nervous system (CNS), including the diencephalon (Bradley et al., 2006; van Eekelen et al., 2003). Tracing of Tal1-expressing neurons in the r-Th indicates that this progenitor pool will form the IGL and, to a minor extent, part of the ventral lateral geniculate (vLGN) (Jeong et al., 2011). Much less information is available regarding the embryonic origin of other nuclei of the SVS, but GABAergic transcription factors that, like Tal1, are expressed in the r-Th have also been described in the posterior pretectum, notably Helt (alias Mgn) and Sox14. Helt encodes a bHLH-Orange transcription factor with an essential role in differentiation of GABAergic neurons in the midbrain (Guimera et al., 2006a, 2006b; Nakatani et al., 2004). Sox14 is a member of the SRY-related HMG box class of transcription factors and it is thought to act as a transcriptional repressor to control lineage fate decisions (Hargrave et al., 2000; Hashimoto-Torii et al., 2003; Uchikawa et al., 1999).

In this Article, we identify Sox14 as a marker for all nuclei of the SVS and show that its expression is required to drive development of a functional network supporting light-entrained circadian behaviors. We provide evidence on the common developmental origins of the SVS from two related neuronal progenitor domains, one in the r-Th and the other in the pretectum. Furthermore, we describe how sequential waves of tangential migration convert the simple organization of the two progenitor territories into the complex architecture of the SVS. This research redefines the role of the SVS as an important regulator of circadian behaviors.

### **RESULTS**

## Sox14 Is Expressed by a Subset of GABAergic Neurons in the Diencephalon

Expression of proneural bHLH transcription factors in the diencephalon defines territories with a determined neurotransmitter fate. Expression of Neurog2 in the rostral pretectum, caudal thalamus, and zona limitans intrathalamica (ZLI) defines diencephalic regions with an excitatory fate (Figures 1A and 1B). By contrast, expression of the bHLH transcription factor Asc/1 defines the caudal pretectum, rostral thalamus, and prethalamus as having an inhibitory fate (Figures 1A and 1B). Upon exiting the cell cycle, neuronal progenitors upregulate expression of transcription factors that are predictive of their nuclear identity. Lhx9-positive neurons contribute to all thalamic nuclei projecting to the cortex (Figures 1A and 1B). Dlx2-positive neurons form prethalamic nuclei including the reticular nucleus of the thalamus and the ventral part of the LGN complex (vLGN) (Figures 1A and 1B).

We describe a neuronal population in the r-Th and caudal pretectum defined by the hierarchical expression of three transcription factors. This population arises in the Ascl1-positive progenitor domain, progressing from an early proliferating cell type expressing Helt to its most differentiated progeny expressing Sox14. Upon Helt downregulation and before Sox14 induction, this population also activates expression Tal1 (Figures 1C, 1E, and 1F).

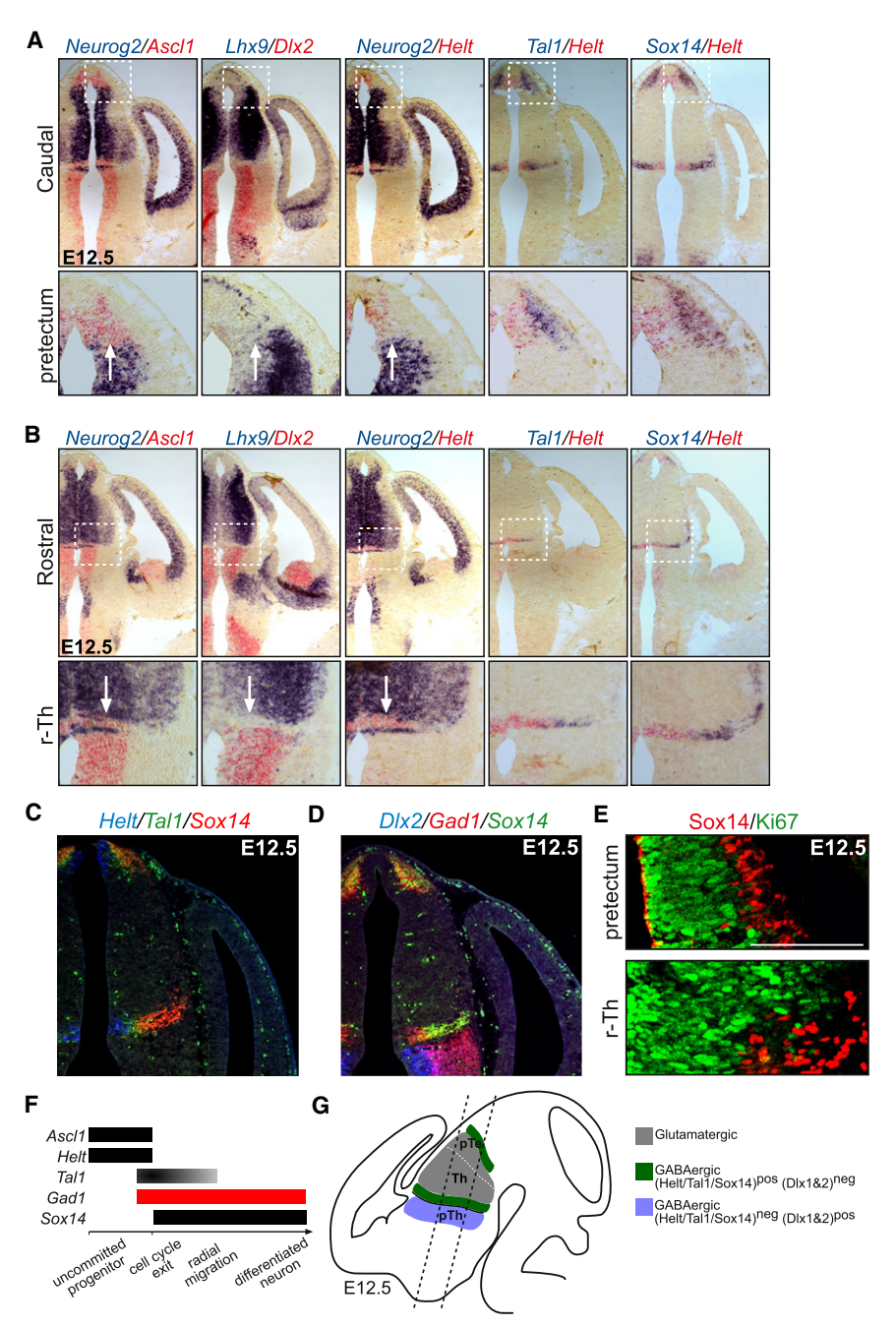
Colabeling of the embryonic day (E) 12.5 diencephalon with Dlx2, Sox14, and Gad1 indicates that GABA-synthesizing neurons arise from either the Dlx2-positive population or Sox14-positive population (Figures 1D and 1G). We therefore conclude that all Dlx2-negative GABAergic neurons in the diencephalon arise from the Helt-, Tal1-, and Sox14-positive population and that Dlx2 expression or lack of it defines two alternative GABAergic subtypes.

### Sox14 Expression Underlies Development of the SVS

The onset of Sox14 expression correlates with cell-cycle exit in cells that have already initiated transcription of the Gad1 gene (Figures 1D-1F). Sox14 expression is maintained during embryogenesis but is progressively lost within the first 3 weeks after birth (data not shown). By contrast, Helt is only transiently expressed from the onset of neurogenesis up to E14.5 and Tal1 is expressed in intermediate progenitors but not in the most differentiated stages (Figures 1A-1C and 1F). Therefore, to further study the development and function of this diencephalic neuronal population, we took advantage of a knockout (KO) mouse in which the Sox14 coding sequence is replaced by the cDNA for eGfp by homologous recombination (Crone et al., 2008). The heterozygote Sox14gfp/+ is virtually a wild-type (WT) animal and is therefore a useful tool to study Sox14-expressing neurons during their normal development. From the onset of neurogenesis, green fluorescent protein (GFP)-expressing cells are visible in two stripes extending transversely across the diencephalon, coinciding with the r-Th and the caudal pretectum (Figures 2A and 2B). In the hypothalamic region, GFP is visible in the future ventromedial hypothalamus (VMH) and in the medial preoptic area (MPO) (Figures 2B and 2C and data not shown). Several differences in marker expression between the r-Th/pretectal domain and the hypothalamic domain of Sox14 expression, including the Helt and Tal1 transcription factors and the neurotransmitter markers Gad1 and Vglut2, suggest that the hypothalamic Sox14-positive domain follows an altogether different developmental program and was not considered further.

To assess the fate of pretectal and thalamic Sox14-positive cells, we followed their location during nucleogenesis from stage E14.5 to postnatal day (P) 2. By E16.5, Sox14 cells form welldefined clusters in the pretectum, thalamus, and prethalamus. The most rostrodorsal cluster of Sox14 cells is located next





to the lateral habenula (LHa, labeled by *Prokr2* expression) (Figures 2C and 2D and see Figure S1 available online). This cluster extends in a caudoventral direction along the thalamus-pretectum border to form the nucleus posterior limitans (PLi). In the pretectum, a cluster of *Sox14*-positive cells occupies the area of the OPN and of the commissural pretectal area (CPA, expressing *Npy*; Figure S1) (Borostyánkoi-Baldauf and Herczeg, 2002; Prichard et al., 2002); from the OPN, *Sox14*-positive cells extend laterally in the thin layer of cells that make up the nucleus of the optic tract (NOT) (Figures 2C and 2D). In a more ventral location, *Sox14*-positive cells cluster at the

Figure 1. GABAergic Neurogenesis in the Diencephalon

(A and B) Posterior pretectum (A), r-Th, and prethalamus (B) express the panGABAergic proneural bHLH marker *Ascl1* and are negative for the glutamatergic markers *Ngn2* and *Lhx9* (arrows). (A–D) Pretectal and rostral thalamic GABAergic progenitors express *Helt*, *Tal1*, and *Sox14* but lack

progenitors express *Helt*, *Tal1*, and *Sox14* but lack expression of *Dlx2*.

(C and D) Confocal images of fluorescent ISH on consecutive sections.

(C and F) *Helt*, *Tal1*, and *Sox14* are expressed sequentially in differentiating rostral thalamic and pretectal neuronal progenitors.

(E) Sox14 is not coexpressed with the cell-cycle marker Ki67. Confocal images of IHC are shown. (F) Onset of marker gene expression within the pretectal and rostral thalamic domains in relationship to cellular differentiation.

(G) Schematic representation of the main progenitor domains across the prethalamus, thalamus, and pretectum. All sections cut coronally at 14  $\mu$ m from E12.5 embryos. Scale bar represents 100  $\mu$ m.

thalamus-prethalamus border to form the IGL (labeled by *Npy* expression) with scattered cells in the vLGN (Figures 2C, 2D, and S1). As at E12.5, all *Sox14*-positive clusters coexpress the GABAergic marker *Gad1* (Figure S1).

GFP-positive axons of *Sox14*-expressing nuclei extend into the hypothalamus to reach and surround the SCN (Figure 2C). GFP-positive axons also extend between the IGL and the PLi and between the PLi and the OPN and CPA (Figures 2C and 2D). Based on their anatomical location and on their cross-connections, we define the pretectal and thalamic domains of *Sox14*-expressing cells as being part of the SVS.

To show that *Sox14*-expressing cells are part of the non-image-forming circuit originating with ipRGCs, we followed the retrograde transsynaptic spread of the Bartha strain of the pseudorabies virus (PRV152tdTomato). Upon injection in the

eye chamber, PRV152 spreads through the parasympathetic circuit controlling the PLR, eventually reaching ipRGCs in the contralateral eye 72 hr after infection (Figure 2F) (Pickard et al., 2002; Viney et al., 2007). We have found that at P3, pups are old enough to survive the procedure and expression from the Sox14 locus is still detectable, albeit at reduced levels and in fewer cells than at P2. Colabeling of GFP and tdTomato highlighted several Sox14-positive cells that contained viral particles within the OPN, CPA, and IGL (Figure 2E). In contrast, hypothalamic nuclei that are also part of the PLR circuit only contained viral particles but no GFP-expressing cells (SCN and



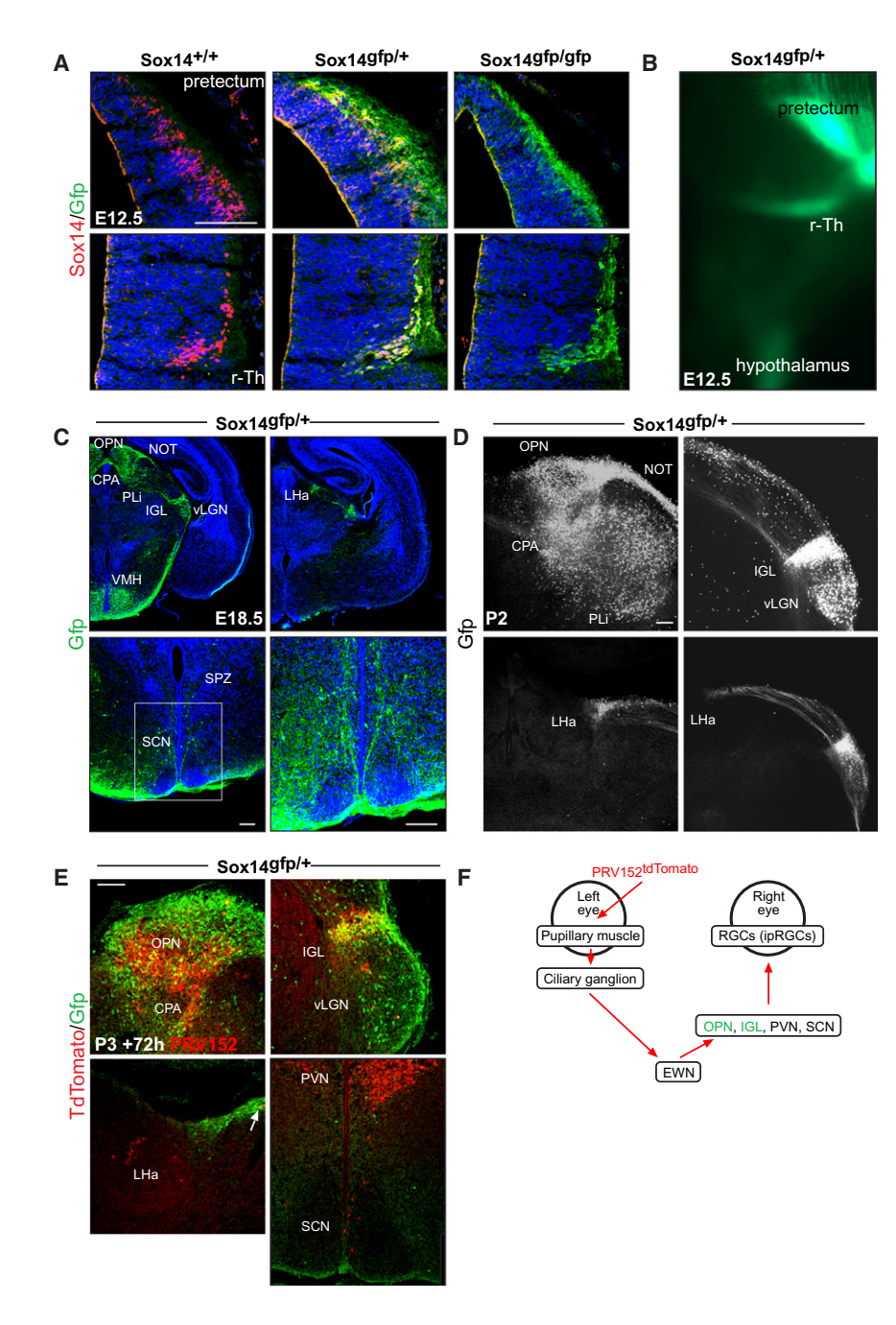


Figure 2. Sox14 Is Expressed in All Nuclei of the SVS, but Not in the SCN

- (A) Expression of Gfp from the Sox14 locus results in the knockout of endogenous Sox14. GFP expression replicates that of the wild-type allele.
- (B) Diencephalic territories expressing Sox14 visualized by GFP fluorescence on a dissected brain at E12.5: lateral view, rostral to the left.
- (C) Immunohistochemistry for GFP localization in the Sox14<sup>gfp/+</sup> brain at E18.5. High-gain confocal images of GFP expression at the level of the SCN and SPVZ. GFP-positive axons surround the SCN along the optic nerve at the chiasm.
- (D) Confocal z stacks on thick sections of short fixed, unstained P2 brains; major components of the SVS colocalize with GFP-expressing regions. (E) Confocal images of the OPN, IGL LHa, SCN, and PVN in  $Sox14^{gfp/+}$  brains 72 hr after PRV152tdTomato injection in the left eye.
- (F) Simplified representation of the transsynaptic retrograde spreading of the PRV152 virus along the PLR circuit. All sections are coronal and cut at 14  $\mu$ m, except for (D) cut at 70  $\mu$ m and (E) cut at 25  $\mu m$ . Scale bar represents 100  $\mu m$ . See also related Figure S1.

the LHa (Figure 3A). Given that no progenitor domain other than the ones we described at E12.5 arises at this location, we supposed that GFP-positive cells move to the LHa and PLi by tangential migration.

To test this hypothesis, we performed live time-lapse imaging on Sox14gfp/+ diencephalic explants in culture. GFPpositive cells are first seen migrating tangentially from the r-Th toward the pretectum at E12.5 (Figures 3B and 3C; Movie S1). Migration starts in the ventralmost part of the thalamus and moves dorsally, eventually concerning only the dorsalmost tip of the GFP-positive r-Th at E14.5 (Figures 3B and 3C; Movie S3). By E15.5, all caudally migrating cells have reached their destination at the border between thalamus and pretectum and at the LHa and this first caudodorsal wave of tangential migration is com-

pleted. At E14.5, the rostral thalamic pool of GFP-positive cells initiates a new wave of tangential migration in a rostroventral direction to colonize the developing vLGN (Figures 3B and 3C; Movie S4).

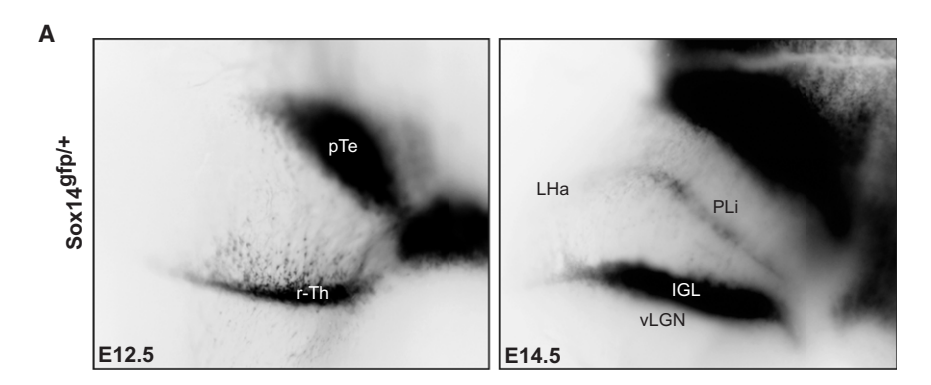
In summary, we define the rostral thalamic domain of Sox14-expressing cells as a source of tangentially migrating GABAergic neurons that form nuclei of the SVS at the thalamus-epithalamus border (next to the LHa), at the thalamuspretectum border (PLi), and in the vLGN. The bulk of the Sox14-positive cells does not migrate tangentially and instead forms the IGL (Figure 3A). We consider the PLi and the region

paraventricular nucleus [PVN]) (Figure 2E). We also noticed very few and isolated viral particles in the LHa, sometimes coexpressed with the Sox14-expressing cells in the region (Figure 2E).

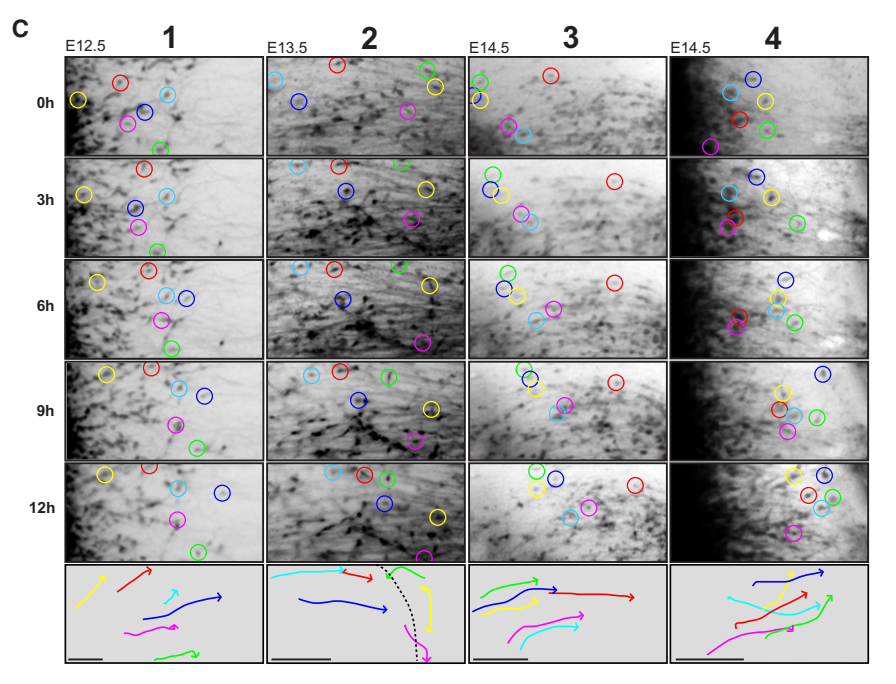
## The Presumptive IGL Is a Source of Tangentially **Migrating Neurons**

Examination of the Sox14gfp/+ diencephalon at E12.5 did not show GFP-expressing cells at the thalamus-pretectum border or next to the habenula (Figure 3A). By contrast, at E14.5, GFP-positive cells are visible at the future PLi and extend toward









lateral to the LHa a continuous structure that shares with the IGL and part of the vLGN a common origin. In the pretectum, Sox14positive cells coalesce in the CPA that continues laterodorsally with the OPN. Minor tangential migration from this region results in spreading of Sox14-positive cells along the NOT and scattered throughout the anterior pretectum (Figure 2C). Some pretectal Sox14-positive cells also appear to reach the PLi (Figure 3C; Movie S2).

Figure 3. Sox14-Positive Neurons Migrate Tangentially from the Presumptive IGL to Form Other Nuclei of the SVS

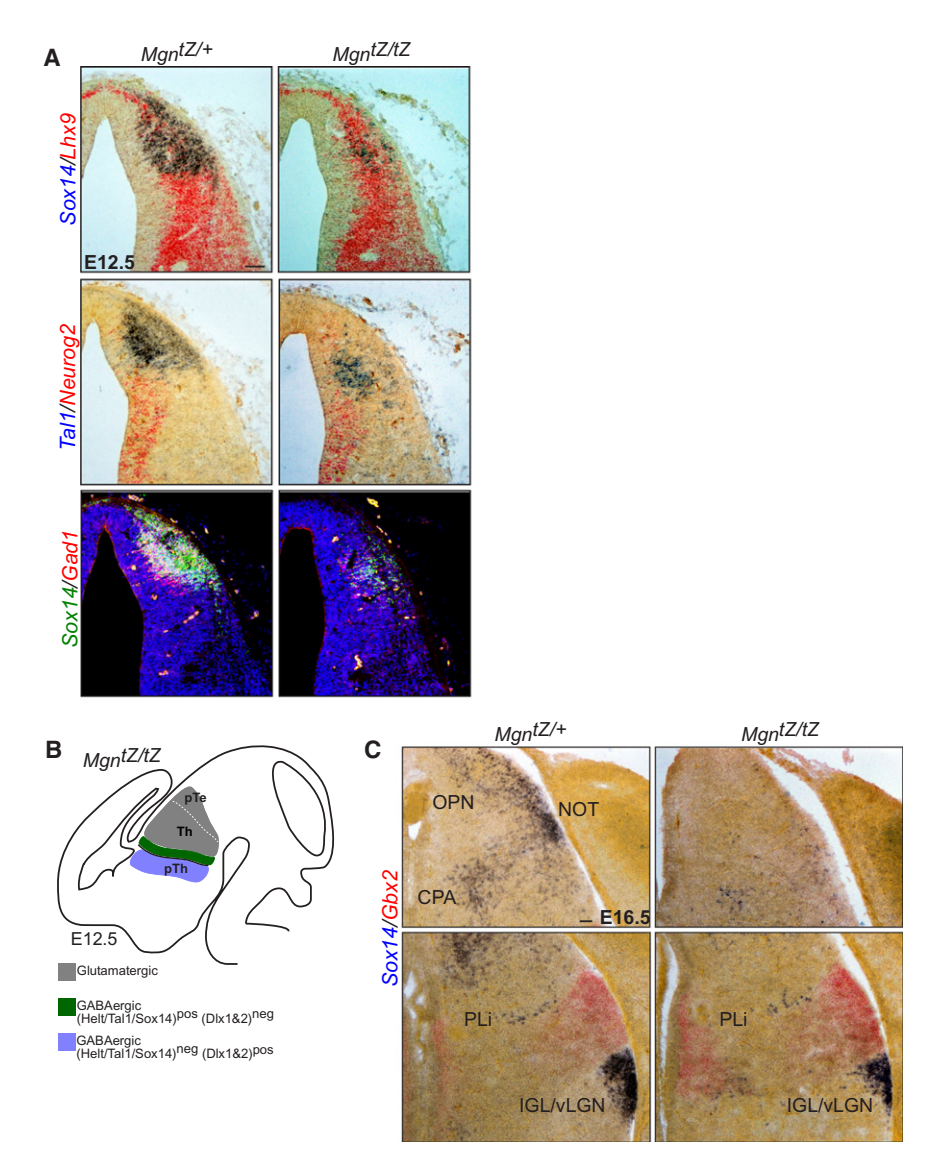
(A) Lateral view of forebrain explants from Sox14<sup>gfp/+</sup> at E12.5 and E14.5 under fluorescence. Tangentially migrating neurons are visible by E12.5. At E14.5, GFP-positive cells have condensed at the thalamic-pretectal border to form the nucleus PLi, ongoing migration involves the rostral-/dorsalmost region next to the LHa. (B and C) Consecutive waves of tangential migration in a schematic view of the mouse brain from E12.5 to E14.5 (B); numbered frames correspond to areas in (C). Selected frames at 3 hr intervals of time-lapse recordings of migrating cells from live explants (C); regions as summarized in (B). Six color-coded cells per region were tracked and their path redrawn to generate representative migratory tracks. Frame 2 shows pretectal cells (yellow and green) also contributing to the PLi (dotted line) (C). See also related Movies S1, S2, S3, and S4.

## Helt Is Required for Induction of **SVS Development in the Pretectum**

Gene expression analysis and live imaging indicate that nuclei of the SVS arise from two progenitor domains, the r-Th and the caudal pretectum. We identified Helt as an early lineage-specific transcription factor expressed by both pools. We therefore investigated whether Helt function is required for SVS development. Analysis of the diencephalon at E12.5 in the Helt knockout mouse (MgntZ/tZ) revealed a strong downregulation of Sox14. Tal1, and the GABAergic marker Gad1 in the pretectum, but not in the r-Th (Figures 4A and 4B and data not shown). By E16.5, Sox14 is nearly absent from the pretectum, with only a few cells visible in the presumptive CPA (Figure 4C). In contrast to Helt function in the midbrain, where it acts to promote the GABAergic fate by suppressing the alternative glutamatergic lineage determinants Neurog1 and Neurog2 (Nakatani et al., 2007), progenitors in the Mgn<sup>tZ/tZ</sup> pretectum do not upregulate Neurog2 expression (Figure 4A). Yet, the alternative lineage marker Lhx9

expands into the posterior pretectum, suggesting that  $Mgn^{tZ/tZ}$ pretectal progenitors have switched to an excitatory fate (Figure 4A). The failure to induce the genetic program underlying SVS development in the pretectum, but not in the r-Th, gave us an opportunity to further investigate the contribution of these two domains to the nucleus PLi that forms at the boundary between thalamus and pretectum. At E16.5, the MgntZ/tZ diencephalon displays a normal accumulation of Sox14-positive cells





at the thalamus-pretectum border (Figure 4C), further confirming that this segment of the SVS develops largely from the r-Th via tangential migration, with only minimal contribution from the pretectum.

## Dlx1 and Dlx2 Are Required in the Developing vLGN to Suppress the IGL Fate

At E12.5, rostral thalamic Sox14-positive GABAergic neurons abut the bulk of GABAergic Dlx2-positive neurons of the prethalamus (Figure 1D). We hypothesized that Sox14-positive and Dlx2-positive cells are two alternative GABAergic subtypes. To test whether an epistatic relationship exists between the cell types, we investigated the development of the Sox14-positive population in a mouse mutant for Dlx2 and for the similarly expressed Dlx1 genes (Dlx1/2<sup>2KO</sup>). This double knockout mouse displays strongly impaired neuronal differentiation in the ventral telencephalon and prethalamus, with incomplete maturation and impaired migration of GABAergic progenitors (Anderson

Figure 4. The Transcription Factor Helt Is Required to Induce Sox14 Expression and SVS Formation in the Pretectum but Not in the Thalamus

(A) Helt expression in the posterior pretectum is required to differentiate Tal1-, Sox14-positive progenitors. Alternative lineages in the anterior pretectum and thalamus are labeled by Lhx9. The glutamatergic proneural gene Neurog2 is not induced in the pretectum of Helt-deficient mice  $(Mgn^{tZ/tZ}).$ 

(A and C) GABAergic differentiation and SVS nuclei formation is reduced in the pretectum of Heltdeficient mice (Mgn<sup>tZ/tZ</sup>), visualized by expression of the panGABAergic marker Gad1 and the SVS marker Sox14.

(B) The pretectal-specific effects of Helt loss are summarized.

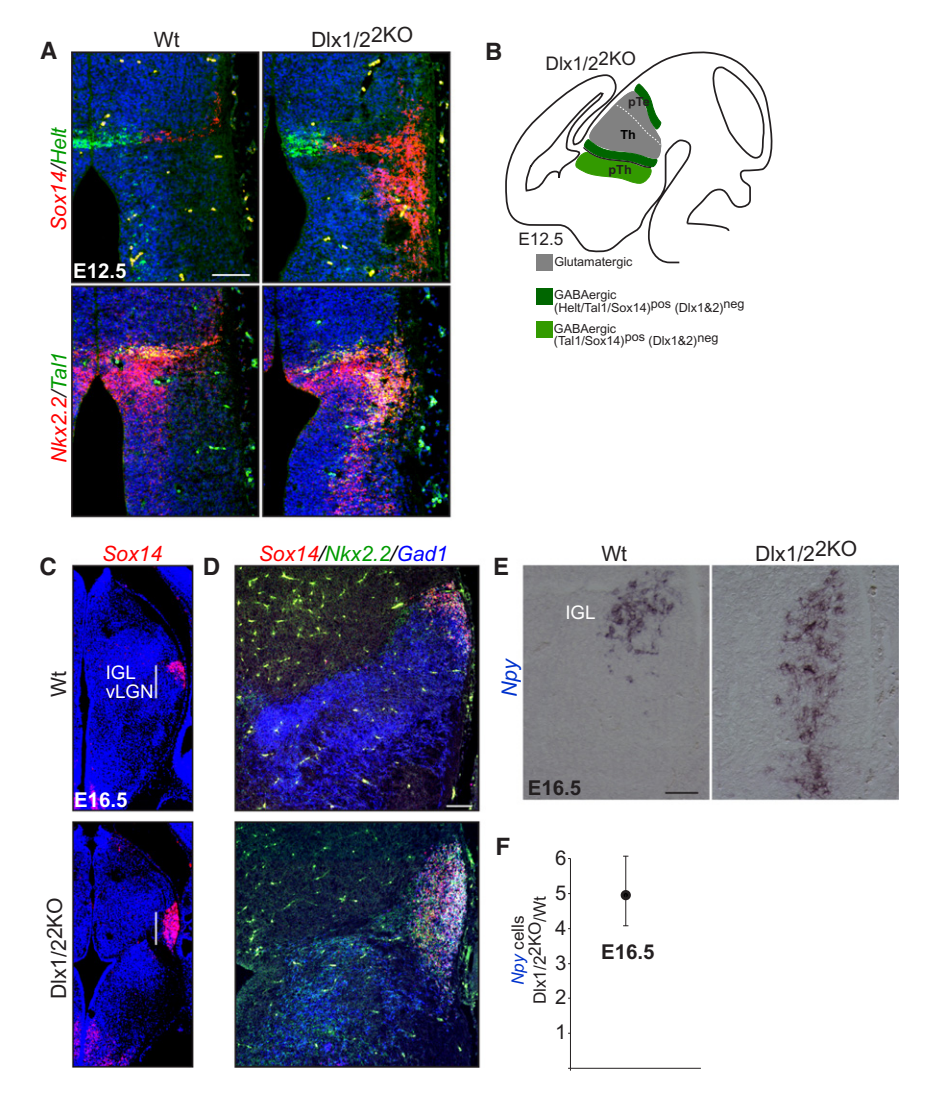
(C) The PLi of Helt-deficient mice is still populated by Sox14-positive cells, indicating that the developing IGL is the main source of tangentially migrating neurons for this nucleus. (A) and (C) are ISH on coronal sections at 14  $\mu m$  thickness. Scale bar represents 100 μm.

et al., 1997; Cobos et al., 2005). At E12.5 in the  $Dlx1/2^{2KO}$ , Tal1 and Sox14 are ectopically induced in the prethalamus, mirroring their position in the r-Th (Figures 5A and 5B). Interestingly, the ectopic induction of Tal1 and Sox14 did not correlate with ectopic expression of Helt in the cycling progenitor domain of the prethalamus, an observation that helps place Helt function at an earlier stage than Dlx2 (Figures 5A and 5B).

By E16.5 of normal development, most Dlx2-positive GABAergic neurons in the prethalamus have formed the reticular nucleus, while those arising closer to the ZLI form the vLGN. As shown

above, the vLGN is invaded at E14.5 by Sox14-expressing GABAergic neurons from the r-Th (Figures 3B and 3C; Movie S4). This results in the intermixing of Sox14-positive neurons within the largely Dlx2-expressing vLGN. However, in the double  $DIx1/2^{2KO}$  mouse, the entire vLGN is occupied by Sox14-positive neurons (Figures 5C and 5D). We then asked whether ectopic Sox14-positive neurons in the vLGN acquire their normal GABAergic fate. Indeed the panGABAergic marker Gad1 is highly expressed in these cells despite lack of expression of Dlx1 and Dlx2 (Figure 5D). To assess whether these ectopic neurons have also acquired a full IGL character, we measured expression of the IGL marker Npy. Ectopic Sox14 cells in the vLGN express a high level of Npy, resulting in a  $\sim$ 5-fold increase of Npy-positive cells in the combined IGL/vLGN region compared to control littermates (Figures 5E and 5F). We therefore conclude that ectopic Sox14-positive cells are true IGL cells and that Dlx1 and Dlx2 act to suppress IGL fate in the vLGN. Concomitant ectopic induction of Helt is not required for the





acquisition of IGL marker expression or GABAergic fate, in agreement with the lack of any detectable phenotype in the rTh of Mgn<sup>tZ/tZ</sup> mice. This observation also rules out the possibility that Dlx1 and Dlx2 act as prepatterning genes before the onset of neurogenesis and that in their absence prethalamus is converted into thalamus. The ectopic IGL lineage in the prethalamus overlaps with expression of the Shh-induced gene Nkx2.2 (Figures 5A and 5D). This suggests that on both sides of the ZLI, Nkx2.2 specifies GABAergic progenitors that differentiate either as IGL or vLGN neurons and that this decision is regulated at least in part by the transcription factors DIx1 and DIx2.

## Sox14-Deficient Neurons Retain Their GABAergic Fate, but Fail to Colonize the vLGN

Our analysis of Sox14 expression defines this gene as a useful marker for the developing SVS. Expression of Sox14 is controlled by three key regulators of GABAergic development at different locations in the diencephalon: positive regulation by Helt in the pretectum and negative regulation by Dlx1&2

## Figure 5. The Transcription Factors Dlx1 and Dlx2 Suppress IGL Fate within Common **GABAergic LGN Progenitors**

- (A) Confocal fluorescent ISH of SVS-lineage markers Helt, Tal1, and Sox14 and their ectopic induction within the Nkx2.2<sup>high</sup> domain of the prethalamus of Dlx1/2<sup>2KO</sup> mice at E12.5.
- (B) Lateral view of the spatial organization of GABAergic progenitor domains in the embryonic diencephalon.
- (C) Ectopic Sox14 expression in the vLGN of Dlx1/22KO mice at E16.5.
- (D) Confocal images of the GABAergic markers Gad1 in combination with the SVS marker Sox14 and the regional marker Nkx2.2.

(E and F) Representative image of ectopic IGL cells in the IGL/vLGN complex of Dlx1/22KO mice at E16.5 (E) and quantification of the increase in Npyexpressing cells of the mutant over the control mice at E16.5 (average change, 5.0-fold; max 6.2fold; min 4.0-fold; n = 3-3) (F). All sections cut coronally at 14  $\mu m.$  Scale bar represents 100  $\mu m.$ 

in the prethalamus. Tal1 was previously shown to be required for survival of differentiating GABAergic progenitors.

We then went on to investigate whether Sox14 is also required, downstream of Helt and Tal1, to differentiate functional GABAergic neurons of the SVS. Expression of Gad1 in the Sox14gfp/gfp animals is comparable to Sox14gfp/+ littermates. suggesting that Sox14 is not required for the acquisition of the inhibitory phenotype (data not shown).

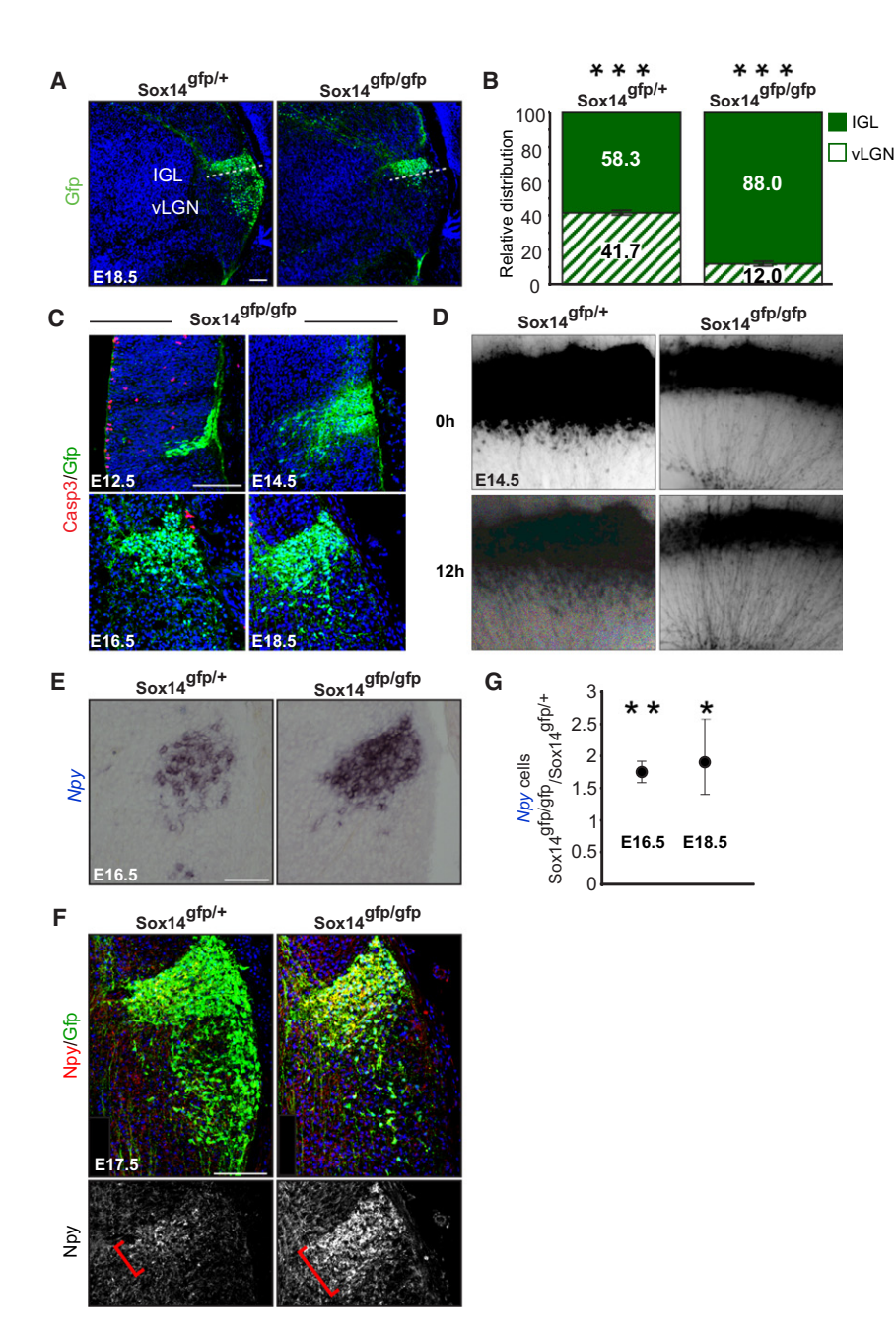
We then assessed whether the positioning of SVS nuclei was affected in the mutant. However, the OPN, NOT, and CPA in the pretectum formed nor-

mally, as did the IGL and its derivative structures at the LHa and PLi (Figure 6B and data not shown). Importantly, the geniculohypothalamic projection to the SCN is also visible (Figure S2).

In contrast to the normal distribution of those SVS neurons, GFP-positive cells were largely absent from the vLGN of  $Sox14^{gfp/gfp}$  animals (Figures 6A and 6B). To investigate whether this lack was due to increased apoptosis at the IGL, we measured activation of Caspase-3 in Sox14<sup>gfp/gfp</sup> and Sox14<sup>gfp/+</sup> littermates between E12.5 and E18.5, when cells migrate into the vLGN from the IGL. We could not detect any increase in apoptosis in the mutant diencephalon (Figure 6C). We therefore hypothesized that in the absence of Sox14, IGL cells lose the ability to migrate into the vLGN. Time-lapse analysis confirmed the migratory defect in IGL cells in the  $Sox14^{gfp/gfp}$  mouse (Figure 6D; Movies S5 and S6).

Having found that in the absence of Sox14 expression the developing IGL fails to colonize the vLGN, we postulated that those additional neurons now retained within the presumptive IGL complete their differentiation to become IGL neurons by





upregulating Npy expression. Counting of Npy-expressing cells in the Sox14gfp/gfp and control littermates reveals a significant increase in Npy-positive cells, consistent with our hypothesis (average increase: 1.7-fold at E16.5 and 1.9-fold at E18.5) (Figures 6E-6G).

## The Phase of the Circadian Rhythm of Sox14-Deficient **Mice Is Not Entrained to Light**

The IGL, together with OPN and SCN, is a major target of ipRGCs. The IGL is also the site of initiation of the geniculohypothalamic tract. This tract is a major contributor of Npy-positive afferents to the SCN and SPVZ, where release of Npy induces phase shifts of the circadian rhythm. The observation that

### Figure 6. Sox14-Deficient IGL Neurons Fail to Colonize the vLGN

(A) IHC of GFP localization in the IGL and vLGN of Sox14gfp/+ and Sox14gfp/gfp embryos; by E18.5, the vLGN of mutant mice is largely devoid of GFPpositive cells.

(B) Quantification of the relative distribution of GFP-positive cells between IGL and vLGN in Sox14gfp/+ control and Sox14gfp/gfp mutant embryos; vLGN:  $Sox14^{gfp/+}$  41.7 ± 1.4;  $Sox14^{gfp/gfp}$  $12.0 \pm 1.5$  (average  $\pm$  SEM; t test: p < 0.0001;

(C) Lack of activated Caspase-3 expression in GFP-positive cells of the developing IGL. Positive signals from apoptotic cells are detectable in other areas of the sections (data not shown).

(D) Selected frames at time point 0 and after 12 hr from time-lapse imaging on tissue explants from Sox14gfp/+ control and Sox14gfp/gfp mutant embryos at E14.5; lateral view, rostral to the left.

(E) Representative images of the IGL in control Sox14gfp/+ and Sox14gfp/gfp embryos at E16.5 labeled by the IGL-specific neuromodulator Npy (ISH).

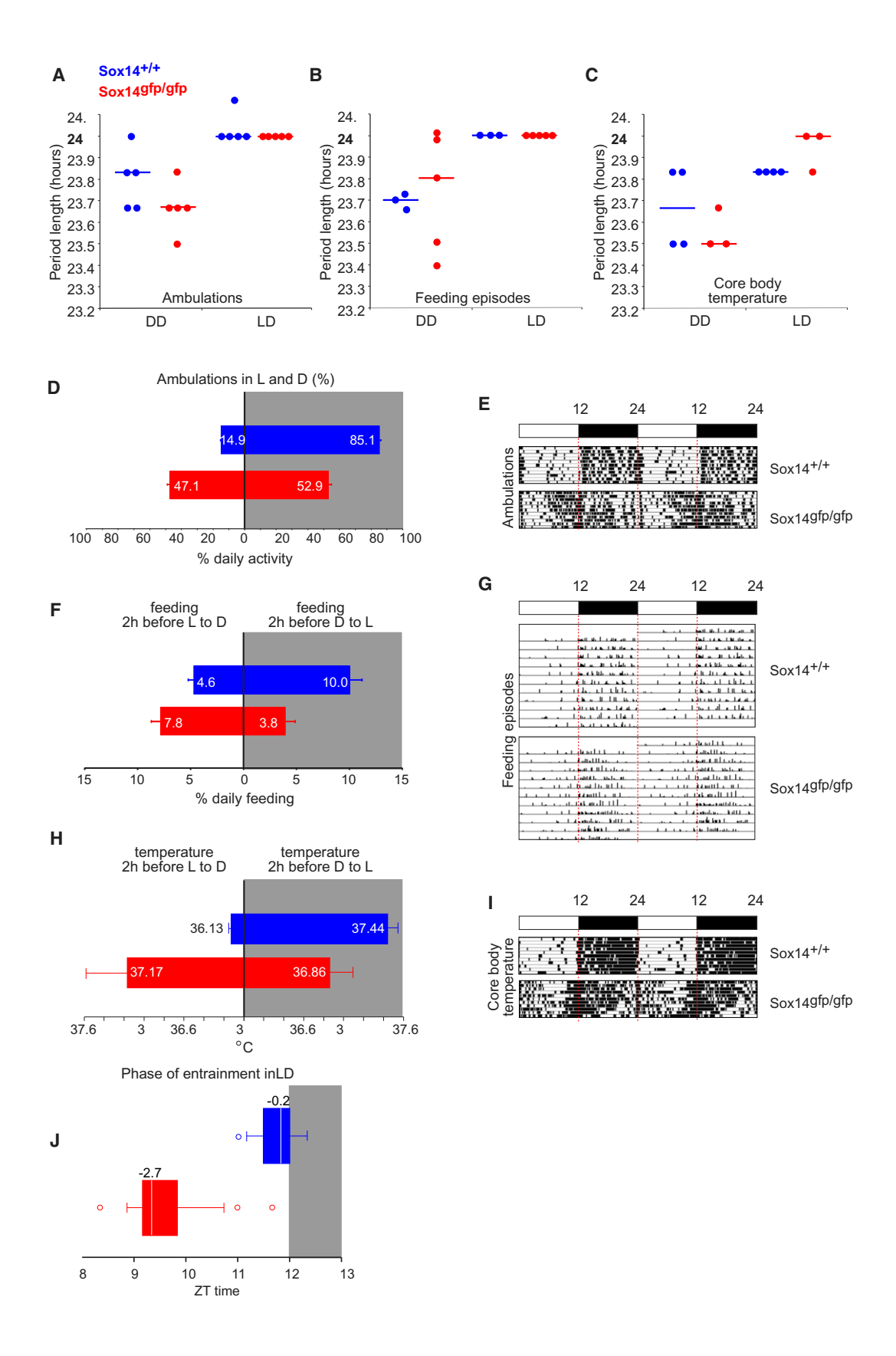
(F) Representative confocal z projections of the IGL and vLGN in Sox14gfp/+ and Sox14gfp/gfp embryos at E17.5 labeled by the IGL-specific neuromodulator Npy (red) in combination with GFP (areen) (IHC).

(G) Quantification of the increase in Npy-expressing cells at the IGL of Sox14gfp/gfp embryos E16.5: 1.7 (min 1.6, max 1.9), E18.5: 1.9 (min 1.4, max 2.6); fold change ± min and max range; t test: p < 0.001 at E16.5 and p = 0.01 at E18.5; n = 4 per genotype, per embryonic stage. All sections cut coronally at 14  $\mu m$ . Scale bar represents 100  $\mu m$ . See also related Figure S2 and Movies S5 and S6.

Sox14 is required to control the distribution of r-Th progenitors between the presumptive IGL and vLGN domains and the resulting increase in Npy-positive IGL neurons in the Sox14gfp/gfp mutant mouse embryo led us to investigate whether the circadian clock of these mice would be compromised in its ability to entrain to a light:dark (LD) cycle. Notably, Sox14 is never expressed in

the retina, and ipRGCs form normally in the Sox14gfp/gfp mutant mouse (data not shown). To verify that neural signals from the retina to SVS neurons and the SCN core are functional, we measured induction of the immediate early gene c-fos in Sox14gfp/gfp and control mice before and after acute light exposure (aL) (Figures S3A and S3B). During the dark period, the SCN and the SVS do not express c-Fos, but the gene is strongly upregulated 1 hr after light exposure during the subjective dark phase (Figure S3B). We could detect no major differences in c-Fos levels between Sox14gfp/gfp and control mice upon acute light exposure (Figure S3B). We conclude that Sox14gfp/gfp mice have not lost the ability to transduce signals from the retina to their diencephalic targets.







To assess whether Sox14gfp/gfp mice have a functional SCN capable of generating an endogenous circadian rhythm, we measured the period of three well-known circadian behaviors and physiological responses that are controlled by the SCN: motor activity, feeding episodes, and core body temperature. The intrinsic period of the clock becomes apparent under constant dark (DD) conditions. As expected, wild-type mice show a free-running circadian period shorter than 24 hr for all three parameters recorded. Sox14gfp/gfp mice displayed circadian behaviors with a free-running period similar to control mice (Figures 7A-7C) (ambulations: wild-type 23.8, Sox14<sup>gfp/gfp</sup> 23.6; feeding episodes: wild-type 23.7, Sox14gfp/gfp 23.4; core body temperature: wild-type 23.7, Sox14gfp/gfp 23.5; median).

We then reintroduced the light variable with the normal 12 hr light and 12 hr dark (LD) cycle. Under these conditions, both control mice and Sox14gfp/gfp mice adjusted their circadian rhythms in motor activity, feeding, and core body temperature, giving periods very close to 24 hr (Figures 7A–7C) (ambulations: wild-type 24.0, Sox14gfp/gfp 24.0; feeding episodes: wild-type 24.0, Sox14<sup>gfp/gfp</sup> 24.0; core body temperature: wild-type 23.8, Sox14<sup>gfp/gfp</sup> 24.0; median). The retained ability of Sox14<sup>gfp/gfp</sup> mice to respond to environmental light changes was also shown under a 6 hr LD phase advance experiment (Figure S5B). Strikingly though, in Sox14gfp/gfp mice, the phase of all three circadian outputs did not align to the phase of the light cycle (Figures 7E, 7G, 7I, and S5A-S5C). As a consequence of their advanced phase onset, mutant mice displayed increased ambulations during the L phase and decreased ambulations in the D phase compared to controls (Figure 7D) (percentage, daily average ambulations in L phase: wild-type 14.9% ± 0.6%; Sox14<sup>gfp/gfp</sup> 47.1% ± 1.8%; average ± SEM). Similarly, both the onset of feeding and elevation of body temperature were phase advanced. This is shown in Figure 7, which compares feeding (Figure 7F) and body temperature (Figure 7H) in the 2 hr before D onset and the 2 hr before L onset for each genotype (percentage of daily average feeding: wild-type L 4.6% ± 0.6%, D 10.0%  $\pm$  1.2%; Sox14<sup>gfp/gfp</sup> L 7.8%  $\pm$  0.9%, D 3.8%  $\pm$  0.9%; temperature: wild-type L 36.13°C  $\pm$  0.02°C, D 37.44°C  $\pm$  $0.10^{\circ}\text{C}$ ;  $Sox14^{gfp/gfp}$  L 37.17°C ± 0.41°C, D 36.86°C ± 0.23°C; average ± SEM).

The onset of motor activity and feeding in Sox14gfp/gfp mice is variable and fragmented; we therefore looked at the sharper onset in the period for core body temperature rhythm to measure the phase advance in the circadian rhythm of  $Sox14^{gfp/gfp}$  mice (wild-type zeitgeber time [ZT] 11.8 [-0.2 hr advance], Sox14<sup>gfp/gfp</sup> ZT 9.3 [-2.7 hr advance]; median) (Figure 7J).

Overall motor activity is increased in Sox14gfp/gfp mice (approximately 2.5-fold), while there was no significant difference in either total length of feeding episodes (cumulative minutes per day: wild-type: 150.6  $\pm$  10.0,  $Sox14^{gfp/gfp}$ : 168.2  $\pm$ 5.9; average ± SEM) or average core body temperature (wildtype:  $36.7^{\circ}\text{C} \pm 0.06^{\circ}\text{C}$ ,  $Sox14^{gfp/gfp}$ :  $36.9^{\circ}\text{C} \pm 0.2^{\circ}\text{C}$ ; average  $\pm$ SEM). Notably, mutant mice display bouts of strong motor activity consistently localized around the time of D to L transition. Yet, this increased activity is transient and does not change the otherwise independent onset of the 24 hr cycle.

## Sox14-Deficient Mice Do Not Display Light-Dependent **Suppression of Motor Activity**

An important function of ipRGCs is to control the light-dependent suppression of motor activity (negative masking). In this behavioral response, mice in their active phase (during the dark period) display an almost immediate cessation of movement when exposed to bright light. Activity starts again as soon as darkness is reestablished. We used the light paradigm illustrated in Figure 8A, with aL stimulation starting 1 hr into the subjective night (ZT 13) and maintained for the following 2 hr. While control mice had an almost immediate cessation of movement upon aL stimulation, Sox14gffp/gfp mice maintained their activity levels almost unchanged throughout the 2 hr light pulse (percentage of prepulse activity: wild-type: 12.8% ± 3.1%;  $Sox14^{gfp/gfp}$ : 95.2% ± 14.8%; average ± SEM) (Figure 8B). A peculiarity of Sox14gfp/gfp mice is the short-lasting increase in motor activity at each light transition (L to D and D to L). This is particularly evident in the aL stimulation but is also consistently displayed in the circadian recordings under LD conditions for motor activity and for core body temperature (Figures 7E, 7I, S5A, and S5B).

Induction of the PLR completes the set of most studied responses initiated by ipRGCs. We therefore set out to measure the PLR in Sox14gfp/gfp mice. In agreement with the lack of any observable anatomical and neurotransmitter phenotype in the OPN of the Sox14<sup>gfp/gfp</sup> mice, we find that, under the conditions tested, the PLR is unaffected (pupil contraction as percentage of

## Figure 7. Sox14-Deficient Mice Cannot Entrain the Phase of Their Circadian Rhythms to the Light Cycle

(A-C) Period length for ambulations (DD 21 days, LD 14 days, chi-square), feeding events (DD 7 days, LD 7 days, manually calculated with ActogramJ), and core body temperature (DD 14 days, LD 10 days, chi-square) on three independent sets of mice: n = 6-5, n = 3-5, and n = 4-3, respectively. Ambulations: wild-type DD 23.8, LD 24; Sox14gfp/gfp DD 23.6, LD 24.0; feeding episodes: wild-type DD 23.7, LD 24.0; Sox14gfp/gfp DD 23.4, LD 24.0; core body temperature: wild-type DD 23.7, LD 23.8; Sox14<sup>gfp/gfp</sup> DD 23.5, LD 24.0; median.

- (D) Ambulations in the L phase as percentage of the 24 hr period: wild-type 14.9% ± 0.6%; Sox14gfr/gfr/ 47.1% ± 1.8%; average ± SEM; t test: p < 0.001.
- (E) Representative actograms illustrating the phase advance in the circadian ambulation rhythm.
- (F and G) Feeding episodes in the 2 hr preceding each light change expressed as percentage of the 24 hr period: wild-type L 4.6% ± 0.6%, D 10.0% ± 1.2%;  $Sox 14^{gfp/gfp} L 7.8\% \pm 0.9\%, D 3.8\% \pm 0.9\%; average \pm SEM; t test: LD p = 0.004, DL p < 0.001 (F) and relative representative actograms (G), bar height represents the second of the properties of the proper$ length of feeding episodes.
- (H and I) Average temperature in the 2 hr preceding each light transition: wild-type L 36.13°C  $\pm$  0.02°C, D 37.44°C  $\pm$  0.10°C; Sox149fp/gfp mice L 37.17°C  $\pm$  0.41°C, D  $36.86^{\circ}$ C  $\pm 0.23^{\circ}$ C; average  $\pm$  SEM; t test: LD p < 0.001, DL p < 0.001 (H) and representative actograms (I).
- (J) Distribution of phase onset for core body temperature rhythms over 10 consecutive days: wild-type ZT 11.8 (-0.2 hr advance); Sox14gfp/gfp ZT 9.3 (-2.7 hr advance); median and percentile distribution; t test: p < 0.001. See also Figures S3 and S5.



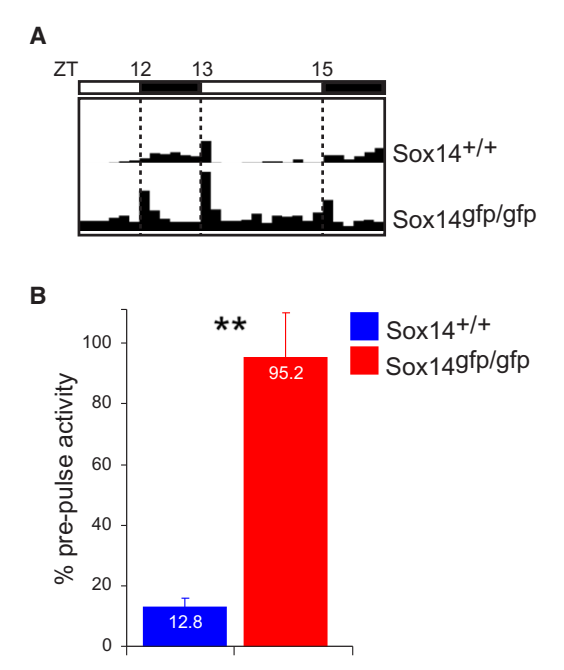


Figure 8. Sox14-Deficient Mice Do Not Display Light-Induced Masking of Motor Activity

(A) Masking of motor activity measured as relative motor activity in 10 min blocks. Light on 1 hr after initiation of the 12 hr dark period; darkness was reintroduced after 2 hr of aL, actograms represent average activity levels; n=6-5.

(B) Residual motor activity during the 2 hr light exposure excluding the first 10 min period, expressed as a percentage of prepulse levels (wild-type  $12.8\% \pm 3.1\%$ ;  $Sox14^{gfp/gfp}$  95.2%  $\pm$  14.8%; average  $\pm$  SEM; t test: p < 0.001; n = 6-5). See also Figure S4.

prepulse area: wild-type 82.2%  $\pm$  2.8%; Sox14 $^{gfp/gfp}$  82.4%  $\pm$  2.7%; average  $\pm$  SEM) (Figure S4).

In summary, our analysis of circadian outputs and light-dependent physiological responses indicates that  $Sox14^{gfp/gfp}$  mice retain the ability to produce an endogenous rhythm (i.e., their endogenous circadian clock is intact), which can be entrained by light to a 24 hr period. Yet, unlike wild-type mice, they are unable to accurately synchronize the phase of their circadian behaviors with the phase of the light cycle. Furthermore, despite being able to sense sudden changes in light intensity (at L to D and D to L, and under aL), they are unable to convert this information into stable entrainment of three circadian responses (motor activity, feeding, and core temperature).

### **DISCUSSION**

Here, we have provided findings on the developmental basis of behavior. By taking a developmental approach, we could describe the stepwise progression from simple to complex that is the underlying base for circuit formation. We have used a loss-of-function approach to define the negative and positive role played by *Dlx1&2*, *Helt*, and *Sox14* in specifying a diencephalic SVS progenitor. By means of live imaging, we followed the early steps required to convert a simple progenitor region

into a complex neuronal network. We mapped Sox14-positive cells within a functionally defined diencephalic network, the SVS, and in a well-known circuit, the non-image-forming circuit initiated by retinal ipRGCs. Finally, we provide a description of the Sox14 loss-of-function phenotype in the mouse and correlate the resulting anatomical defect in the SVS with a specific behavioral outcome.

## The Developmental Defect in SVS Formation in the Sox14 Knockout Mouse and Its Behavioral Correlate

The function of *Sox14* in vertebrates has been obscure. Despite earlier reports suggesting that it may be required for cell fate decisions, we find that in the absence of *Sox14*, SVS neurons retain their GABAergic fate. This could be due to the compensatory function of the closely related family member *Sox21* (Uchikawa et al., 1999). Instead, we find that Sox14 expression is required in the rostral thalamic progenitor pool to induce migration to the vLGN. *Sox14*-deficient neurons that fail to colonize the vLGN are retained in the presumptive IGL, resulting in an increased number of *Npy*-positive cells.

The Sox14 mutant mouse allows for discrimination between the two main sets of ipRGC targets: the SCN and SPVZ, which are Sox14 negative, and the SVS, including IGL and OPN, which is Sox14 positive. All ipRGC axons target the SCN through the excitatory retinohypothalamic tract. This pathway appears normal in Sox14gfp/gfp mice. Consistent with this, their circadian rhythms re-entrain to 24 hr under LD conditions. Yet, ipRGCs extend collaterals into the diencephalon to target Sox14-positive cells in the SVS. Furthermore, new evidence suggests that different classes of ipRGCs preferentially target the IGL and OPN nuclei (Baver et al., 2008; Ecker et al., 2010), Of the two most prominent nuclei in the SVS (IGL and OPN), we find that only the IGL required Sox14 for correct development. Consistent with this, the PLR, which is thought to be mediated by the OPN, is normal in Sox14gfp/gfp mice. The IGL takes an important position in the non-image-forming circuit as it completes a feedback loop with ipRGC-encoded information reaching the SCN first, then the SVS, and, through the IGL (geniculohypothalamic tract), back to the SCN. The observation that the phase of the circadian rhythms of Sox14gfp/gfp mice cannot accurately entrain with the LD cycle provides genetic evidence of the central role that this feedback pathway plays in conferring an additional degree of robustness to retina-encoded photoentrainment. The IGL has been proposed to function as integrator of photic and nonphotic entraining cues. Such putative integrator function finds support in the existence of IGL afferents from hypocretin-expressing neurons of the lateral hypothalamus (Webb et al., 2008) and serotonin-expressing cells in the mesenchephalic raphe complex (Blasiak et al., 2006; Meyer-Bernstein and Morin, 1996). Arousal, induced by forced motor activity during the quiet phase, results in phase advance of the circadian rhythm (Mrosovsky, 1996), which is thought to be mediated by the IGL (Janik et al., 1995; Janik and Mrosovsky, 1994). We used light as the only entraining variable, yet we cannot entirely exclude that  $Sox14^{gfp/gfp}$  mice display increased activation of the arousal system or lower sensitivity threshold to it, which in turn interferes with ipRGC-derived information at the IGL to give rise to the observed phenotype. Importantly, several lines of evidence



have implicated the neuromodulator Npy in phase shifts of the circadian rhythm under both photic and nonphotic conditions (Albers and Ferris, 1984; Biello et al., 1994; Maywood et al., 1997, 2002; Rusak et al., 1989; Shinohara et al., 1993a, IGL-derived geniculohypothalamic fibers GABAergic and release Npy in and around the SCN where Npy levels cycle with two daily peaks at the times of photic transition (Glass et al., 2010; Shinohara et al., 1993a). Hence, our finding that Sox14 is required for normal development of Npy+ cells in the IGL provides a plausible molecular explanation for this behavioral phenotype. Negative masking of motor activity is considered an effect of acute light on the circadian rhythm, yet this phenomenon has been the subject of much less research than photoentrainment and little is known of its molecular and anatomical basis. Here, we implicate Sox 14 as a central player in mediating the acute effect of light on motor behavior.

## DIx1 and DIx2 Specify vLGN Fate at the Expenses of IGL **Fate within Committed Diencephalic GABAergic Progenitors**

Nearly all neurons in the SVS express GABA (Harrington, 1997; Klooster and Vrensen, 1997; Ottersen and Storm-Mathisen, 1984; Radian et al., 1990) and pharmacological manipulations of the GABAergic system change the response of the circadian rhythm to light (Golombek and Ralph, 1994; Ralph and Menaker, 1989). We have defined GABAergic progenitors of the SVS by their sequential activation of three lineage-restricted transcription factors: Helt, Tal1, and Sox14. This GABAergic population is distinguishable from prethalamic GABAergic neurons, which express many of the transcription factors associated with GABAergic neurogenesis in the ventral telencephalon, e.g., Dlx1 and Dlx2, that are not expressed by rostral thalamic cells. The sharp transition between rostral thalamic and prethalamic GABAergic marker expression coincides with the middiencephalic organizer, the ZLI.

At this anatomical location, both developmental programs are exposed to the organizer activity of the ZLI, allowing for fair comparison between the two. Using a loss-of-function approach, we have described how in the absence of Dlx1 and Dlx2, progenitors anterior to the ZLI acquire the fate of those posterior to it. This is an unexpected result because Dlx1 and Dlx2 were not thought to play a role in GABAergic subtype fate decision; rather, they were believed to be required for normal development within the GABAergic lineage.

Our data support a model whereby high Shh-signaling from the ZLI defines a symmetric progenitor domain both rostrally and caudally. This symmetric domain is defined by high Nkx2.2 expression and has a GABAergic fate. Asymmetric interpretation of Shh-signaling within the Nkx2.2high domain induces IGL formation in the rostral thalamic compartment and vLGN formation in the prethalamic compartment. The two programs are antagonistic and removal of Dlx1 and Dlx2 in the vLGN domain is sufficient for the ectopic IGL developmental program to take place. An interesting feature of this model is that the GABAergic subtype switch that takes place as cellular differentiation is well on the way and proneural bHLH genes are being downregulated. Hence, the ectopic induction of IGL progenitors in the vLGN domain does not require a concomitant activation of the thalamic proneural bHLH gene Helt. Helt function highlights an important difference between the rostral thalamic and caudal pretectal GABAergic pools; indeed, Helt is strictly required for Gad1 expression and for the induction of Tal1 and Sox14 in the pretectum but not in the rostral thalamus. In the Mgn<sup>tZ/tZ</sup> mouse, pretectal SVS nuclei are missing, while IGL-derived SVS nuclei are normal, expressing both Tal1 and Sox14.

One of the properties imparted on subpallially derived interneurons by Dlx1 and Dlx2 is the ability to migrate tangentially over long distances to reach their settling position in the cortex and olfactory bulb (Anderson et al., 1997). Similarly, but independent of Dlx gene expression, we describe the pool of rostral thalamic GABAergic progenitors as a highly migratory population, responsible for the distribution of discrete GABAergic nuclei along the rostrocaudal axis of the diencephalon. These migrations crucially convert the single narrow transverse progenitor domain in the rostral thalamus into the complex arrangement of SVS nuclei. Further work will be required to understand how different nuclei within the SVS acquire specific connectivity and the competence to carry out specific tasks within the larger network.

### **EXPERIMENTAL PROCEDURES**

### **Mouse Lines**

All animal procedures were carried out in accordance with the guidelines and protocols approved by the KCL Ethics Committee and the UK Home Office. Sox14gfp/+ mutant mice were generated by L.Z. and T.J. at Columbia University and maintained at KCL. Dlx1;Dlx2 double knockout mice (Dlx1/22KO) were generated and maintained at the UCSF (J.L.R.R.). MgntZ/tZ knockout mice were generated and maintained at the Helmholtz Zentrum München (J.G.).

## **Histological Analysis**

Fluorescent and DAB immunohistochemistry and RNA in situ hybridization on frozen sections were carried out using standard techniques (detailed protocols in Supplemental Experimental Procedures).

## **Intraocular Injection of Virus**

Recombinant PRV152tdTomato was injected through the closed eyelid in the left anterior eye chamber (<1  $\mu$ l) of cold-anaesthetized P3  $Sox14^{gfp/+}$  mice using a glass needle connected to a pressure pump (1-2 pulses, 8 ms, 0.8 bar). Pups were returned to their parents and sacrificed 72 hr later. The entire procedure was carried out in a biosafety level 2 laboratory.

### **Explant Cultures**

Brains from Sox14gfp/+ and Sox14gfp/gfp embryos (E11.5 to E14.5) were dissected out in ice-cold Hank's balanced salt solution (HBSS). The forebrain was cut along the ventral midline in an open book preparation. The telencephalic hemispheres were removed and the explants transferred on millicell culture filters (Millipore, 0.4 µm, 30 mm diameter) with the ventricular side facing upward. Filters were floated on 1 ml of prewarmed and gassed (37°C. 5% CO<sub>2</sub>) Neurobasal medium (Invitrogen), supplemented with 2% Glutamax (Invitrogen), 1% B27 (Invitrogen), and 1% penicillin, 1% streptomycin, and 0.1% HEPES buffer.

### **Time-Lapse Imaging**

Fluorescent protein expression in live tissue explants was imaged using an inverted Nikon fluorescence scope (Eclipse TE2000-U) coupled to an automated heated stage maintained at 37°C. Images (2,000 ms exposure) were taken every 10 min over a 12 hr period (total of 73 time points). Data acquisition was by MetaMorph software (Molecular Devices). Time-lapse movies were assembled and analyzed using ImageJ (NIH, http://rsb.info.nih.gov/ij). Cell



tracing analysis was carried out using the manual tracking plugin for ImageJ. Six representative cells were chosen to represent the general direction of movement. Cell positions were tracked every 3 hr over a 12 hr period and a representative trace was produced.

#### **Circadian Studies**

Adult male and female mice (22–30 g, 4–8 weeks old at the start of the study) were individually housed with food and water ad libitum at room temperature (22°C  $\pm$  2°C) in either a 12 hr:12 hr LD cycle (lights on at 06:00 hr) or in continuous darkness (DD). Room lighting was provided by ceiling-mounted white fluorescent tubes and by white LED strips (200  $\mu\text{W/cm}^2$ ) directly above the mouse cages. Room light level was monitored continuously with an environmental climate monitor (SwiftBase International). Irradiance was measured inside each mouse cage using a Macam PM 203 optical power meter (Macam Photometrics). Cage bedding was changed every 2 weeks.

Activity was measured using a cage-rack photobeam activity system (San Diego Instruments) consisting of a metal photobeam frame with four horizontal infrared beams surrounding each cage. The frames were positioned 1.5 cm above the cage floor and gross movements were recorded (i.e., breaking of adjacent beams). Activity counts in 10 min bins were summed and used to plot actograms and periodograms as shown in Figure 7 using Chronos-Fit Software.

Core body temperature was measured using battery-operated temperature transmitters (TA-F10; Data Sciences International) implanted into the peritoneal cavity under Isoflurane anesthesia 2 weeks before recording began. Temperatures in individually housed mice were recorded for 10 s every 10 min throughout the experiment by a receiver (RPC-1, DSI) placed under each cage. Chronos-Fit Software was used for circadian analysis of core body temperature rhythm.

Feeding episodes were automatically recorded with infrared 1.3 M Pixel USB cameras using the commercially available SecuritySpy software (BenSoftware, http://www.bensoftware.com). Access to food was restricted to the area facing the camera. Recording automatically started when movement was detected in a mask positioned on the food area. Images were captured at 30 frames per second (fps) (320 × 240 pixels). All automatically generated files were inspected individually to discard false positives. Initiation and duration of each event was converted into a suitable input file for the Actogramj (ImageJ plugin, Actogrmj (http://132.187.25.13/actogramj/index. html) using a custom-made script. Feeding events were binned into 10 min units. Bar heights represent duration of feeding events within the 10 min period. Analysis of free-running period length was calculated manually using the "period tool" in Actogramj.

### **Negative Masking Experiments**

WT and  $Sox14^{gfp/gfp}$  mutant mice were housed for 2 weeks before the experiment in a 12 hr:12 hr LD cycle and were shown to be stably entrained by continuous monitoring of activity. A negative masking protocol, similar to one described previously (Thompson et al., 2008), was used. A 3 day experimental protocol of 2 nonpulsed days bracketing a single light pulse day was used; on the pulse day, a 2 hr light pulse was applied starting 1 hr after dark onset (19.00 hr). The light pulse illumination was provided by white LED strips (80  $\mu$ W/cm²) directly above the mouse cages. As activity onset in  $Sox14^{gfp/gfp}$  mutant mice was not synchronized with dark onset, it was not possible to apply the light pulse 1 hr after activity onset as in WT mice. However, the pulse was given at the same clock time (19.00–21.00) as in WT mice; activity recording confirmed this time was during the active period for all of the KO mice.

### **Pupillary Light Reflex**

PLR measurement was carried out at ZT 16 in the dark. Adult wild-type and  $Sox14^{gfp/gfp}$  mice were anaesthetised with Isoflurane and their head immobilized on a stereotaxis apparatus. A 10 s light-pulse (3–5 mW) on the left eye was followed by a 2 min recovery time. PLR was recorded from the right eye with an infrared 1.3 M Pixel USB camera at 10 fps. Pupillary constriction was calculated using ImageJ software by taking the pupillary area immediately prior to light stimulation and 10 s after.

### SUPPLEMENTAL INFORMATION

Supplemental Information includes five figures, Supplemental Experimental Procedures, and six movies and can be found with this article online at http://dx.doi.org/10.1016/j.neuron.2012.06.013.

### **ACKNOWLEDGMENTS**

We would like to thank Kamill Balint and Botond Roska for advice on PRV152-mediated circuit tracing. We are grateful to Giorgio Gilestro, Grant Wray, and Gordon Haggart for their help in setting up the feeding behavioral assay. This work was funded by MRC Programme grant G0601064 to A.L. A.D. is recipient of an EU Marie Curie fellowship.

Accepted: June 1, 2012 Published: August 22, 2012

### **REFERENCES**

Albers, H.E., and Ferris, C.F. (1984). Neuropeptide Y: role in light-dark cycle entrainment of hamster circadian rhythms. Neurosci. Lett. 50, 163–168.

Anderson, S.A., Eisenstat, D.D., Shi, L., and Rubenstein, J.L. (1997). Interneuron migration from basal forebrain to neocortex: dependence on Dlx genes. Science *278*, 474–476.

Baver, S.B., Pickard, G.E., Sollars, P.J., and Pickard, G.E. (2008). Two types of melanopsin retinal ganglion cell differentially innervate the hypothalamic suprachiasmatic nucleus and the olivary pretectal nucleus. Eur. J. Neurosci. 27, 1763–1770.

Berson, D.M., Dunn, F.A., and Takao, M. (2002). Phototransduction by retinal ganglion cells that set the circadian clock. Science 295, 1070–1073.

Biello, S.M., Janik, D., and Mrosovsky, N. (1994). Neuropeptide Y and behaviorally induced phase shifts. Neuroscience 62, 273–279.

Blasiak, T., Siejka, S., Raison, S., Pevet, P., and Lewandowski, M.H. (2006). The serotonergic inhibition of slowly bursting cells in the intergeniculate leaflet of the rat. Eur. J. Neurosci. *24*, 2769–2780.

Borostyánkoi-Baldauf, Z., and Herczeg, L. (2002). Parcellation of the human pretectal complex: a chemoarchitectonic reappraisal. Neuroscience *110*, 527–540

Bradley, C.K., Takano, E.A., Hall, M.A., Göthert, J.R., Harvey, A.R., Begley, C.G., and van Eekelen, J.A. (2006). The essential haematopoietic transcription factor ScI is also critical for neuronal development. Eur. J. Neurosci. *23*, 1677–

Cobos, I., Broccoli, V., and Rubenstein, J.L. (2005). The vertebrate ortholog of Aristaless is regulated by Dlx genes in the developing forebrain. J. Comp. Neurol. 483, 292–303.

Crone, S.A., Quinlan, K.A., Zagoraiou, L., Droho, S., Restrepo, C.E., Lundfald, L., Endo, T., Setlak, J., Jessell, T.M., Kiehn, O., and Sharma, K. (2008). Genetic ablation of V2a ipsilateral interneurons disrupts left-right locomotor coordination in mammalian spinal cord. Neuron *60*, 70–83.

Dkhissi-Benyahya, O., Sicard, B., and Cooper, H.M. (2000). Effects of irradiance and stimulus duration on early gene expression (Fos) in the suprachiasmatic nucleus: temporal summation and reciprocity. J. Neurosci. 20, 7790–7797.

Ecker, J.L., Dumitrescu, O.N., Wong, K.Y., Alam, N.M., Chen, S.K., LeGates, T., Renna, J.M., Prusky, G.T., Berson, D.M., and Hattar, S. (2010). Melanopsin-expressing retinal ganglion-cell photoreceptors: cellular diversity and role in pattern vision. Neuron 67, 49–60.

Edelstein, K., and Amir, S. (1999). The role of the intergeniculate leaflet in entrainment of circadian rhythms to a skeleton photoperiod. J. Neurosci. *19*, 372–380.

Fu, Y., Zhong, H., Wang, M.H., Luo, D.G., Liao, H.W., Maeda, H., Hattar, S., Frishman, L.J., and Yau, K.W. (2005). Intrinsically photosensitive retinal ganglion cells detect light with a vitamin A-based photopigment, melanopsin. Proc. Natl. Acad. Sci. USA *102*, 10339–10344.



Glass, J.D., Guinn, J., Kaur, G., and Francl, J.M. (2010). On the intrinsic regulation of neuropeptide Y release in the mammalian suprachiasmatic nucleus circadian clock, Eur. J. Neurosci, 31, 1117-1126.

Golombek, D.A., and Ralph, M.R. (1994). Inhibition of GABA transaminase enhances light-induced circadian phase delays but not advances. J. Biol. Rhythms 9, 251-261.

Guimera, J., Vogt Weisenhorn, D., Echevarría, D., Martínez, S., and Wurst, W. (2006a). Molecular characterization, structure and developmental expression of Megane bHLH factor. Gene 377, 65-76.

Guimera, J., Weisenhorn, D.V., and Wurst, W. (2006b). Megane/Heslike is required for normal GABAergic differentiation in the mouse superior colliculus. Development 133, 3847-3857.

Güler, A.D., Ecker, J.L., Lall, G.S., Haq, S., Altimus, C.M., Liao, H.W., Barnard, A.R., Cahill, H., Badea, T.C., Zhao, H., et al. (2008). Melanopsin cells are the principal conduits for rod-cone input to non-image-forming vision. Nature 453, 102-105.

Hargrave, M., Karunaratne, A., Cox, L., Wood, S., Koopman, P., and Yamada, T. (2000). The HMG box transcription factor gene Sox14 marks a novel subset of ventral interneurons and is regulated by sonic hedgehog. Dev. Biol. 219, 142-153.

Harrington, M.E. (1997). The ventral lateral geniculate nucleus and the intergeniculate leaflet: interrelated structures in the visual and circadian systems. Neurosci. Biobehav. Rev. 21, 705-727.

Harrington, M.E., and Rusak, B. (1989). Photic responses of geniculo-hypothalamic tract neurons in the Syrian hamster. Vis. Neurosci. 2, 367–375.

Hashimoto-Torii, K., Motoyama, J., Hui, C.C., Kuroiwa, A., Nakafuku, M., and Shimamura, K. (2003). Differential activities of Sonic hedgehog mediated by Gli transcription factors define distinct neuronal subtypes in the dorsal thalamus. Mech. Dev. 120, 1097-1111.

Hatori, M., Le, H., Vollmers, C., Keding, S.R., Tanaka, N., Buch, T., Waisman, A., Schmedt, C., Jegla, T., and Panda, S. (2008). Inducible ablation of melanopsin-expressing retinal ganglion cells reveals their central role in non-image forming visual responses. PLoS ONE 3, e2451.

Hattar, S., Liao, H.W., Takao, M., Berson, D.M., and Yau, K.W. (2002). Melanopsin-containing retinal ganglion cells: architecture, projections, and intrinsic photosensitivity. Science 295, 1065-1070.

Janik, D., and Mrosovsky, N. (1994). Intergeniculate leaflet lesions and behaviorally-induced shifts of circadian rhythms. Brain Res. 651, 174-182.

Janik, D., Mikkelsen, J.D., and Mrosovsky, N. (1995). Cellular colocalization of Fos and neuropeptide Y in the intergeniculate leaflet after nonphotic phaseshifting events. Brain Res. 698, 137-145.

Jeong, Y., Dolson, D.K., Waclaw, R.R., Matise, M.P., Sussel, L., Campbell, K., Kaestner, K.H., and Epstein, D.J. (2011). Spatial and temporal requirements for sonic hedgehog in the regulation of thalamic interneuron identity. Development 138, 531-541.

Johnson, R.F., Moore, R.Y., and Morin, L.P. (1989). Lateral geniculate lesions alter circadian activity rhythms in the hamster. Brain Res. Bull. 22, 411-422.

Jones, E.G. (2007). The Thalamus (New York: Cambridge University Press). Kataoka, A., and Shimogori, T. (2008). Fgf8 controls regional identity in the developing thalamus. Development 135, 2873-2881.

Klooster, J., and Vrensen, G.F. (1997). The ultrastructure of the olivary pretectal nucleus in rats. A tracing and GABA immunohistochemical study. Exp. Brain Res. 114, 51-62.

Lucas, R.J., Douglas, R.H., and Foster, R.G. (2001). Characterization of an ocular photopigment capable of driving pupillary constriction in mice. Nat. Neurosci. 4, 621-626.

Maywood, E.S., Smith, E., Hall, S.J., and Hastings, M.H. (1997). A thalamic contribution to arousal-induced, non-photic entrainment of the circadian clock of the Syrian hamster. Eur. J. Neurosci. 9, 1739-1747.

Maywood, E.S., Okamura, H., and Hastings, M.H. (2002). Opposing actions of neuropeptide Y and light on the expression of circadian clock genes in the mouse suprachiasmatic nuclei. Eur. J. Neurosci. 15, 216-220.

Meyer-Bernstein, E.L., and Morin, L.P. (1996). Differential serotonergic innervation of the suprachiasmatic nucleus and the intergeniculate leaflet and its role in circadian rhythm modulation, J. Neurosci, 16, 2097-2111.

Moore, R.Y., Weis, R., and Moga, M.M. (2000). Efferent projections of the intergeniculate leaflet and the ventral lateral geniculate nucleus in the rat. J. Comp. Neurol. 420, 398-418.

Morin, L.P., and Blanchard, J.H. (1998). Interconnections among nuclei of the subcortical visual shell: the intergeniculate leaflet is a major constituent of the hamster subcortical visual system. J. Comp. Neurol. 396, 288-309.

Morin, L.P., and Blanchard, J.H. (2005). Descending projections of the hamster intergeniculate leaflet: relationship to the sleep/arousal and visuomotor systems. J. Comp. Neurol. 487, 204-216.

Morin, L.P., and Pace, L. (2002). The intergeniculate leaflet, but not the visual midbrain, mediates hamster circadian rhythm response to constant light. J. Biol. Rhythms 17, 217-226.

Mrosovsky, N. (1996). Locomotor activity and non-photic influences on circadian clocks. Biol. Rev. Camb. Philos. Soc. 71, 343-372.

Muscat, L., and Morin, L.P. (2006). Intergeniculate leaflet: contributions to photic and non-photic responsiveness of the hamster circadian system. Neuroscience 140, 305-320.

Nakatani, T., Mizuhara, E., Minaki, Y., Sakamoto, Y., and Ono, Y. (2004). Helt, a novel basic-helix-loop-helix transcriptional repressor expressed in the developing central nervous system. J. Biol. Chem. 279, 16356-16367.

Nakatani, T., Minaki, Y., Kumai, M., and Ono, Y. (2007). Helt determines GABAergic over glutamatergic neuronal fate by repressing Ngn genes in the developing mesencephalon. Development 134, 2783-2793.

Ottersen, O.P., and Storm-Mathisen, J. (1984). GABA-containing neurons in the thalamus and pretectum of the rodent. An immunocytochemical study. Anat. Embryol. (Berl.) 170, 197-207.

Pickard, G.E., Smeraski, C.A., Tomlinson, C.C., Banfield, B.W., Kaufman, J., Wilcox, C.L., Enquist, L.W., and Sollars, P.J. (2002). Intravitreal injection of the attenuated pseudorabies virus PRV Bartha results in infection of the hamster suprachiasmatic nucleus only by retrograde transsynaptic transport via autonomic circuits. J. Neurosci. 22, 2701-2710.

Prichard, J.R., Stoffel, R.T., Quimby, D.L., Obermeyer, W.H., Benca, R.M., and Behan, M. (2002). Fos immunoreactivity in rat subcortical visual shell in response to illuminance changes. Neuroscience 114, 781-793.

Radian, R., Ottersen, O.P., Storm-Mathisen, J., Castel, M., and Kanner, B.I. (1990). Immunocytochemical localization of the GABA transporter in rat brain. J. Neurosci. 10, 1319-1330.

Ralph, M.R., and Menaker, M. (1989). GABA regulation of circadian responses to light. I. Involvement of GABAA-benzodiazepine and GABAB receptors. J. Neurosci. 9, 2858-2865.

Redlin, U., Vrang, N., and Mrosovsky, N. (1999). Enhanced masking response to light in hamsters with IGL lesions. J. Comp. Physiol. A Neuroethol. Sens. Neural Behav. Physiol. 184, 449-456.

Rusak, B., Meijer, J.H., and Harrington, M.E. (1989). Hamster circadian rhythms are phase-shifted by electrical stimulation of the geniculo-hypothalamic tract. Brain Res. 493, 283-291.

Scholpp, S., Delogu, A., Gilthorpe, J., Peukert, D., Schindler, S., and Lumsden, A. (2009). Her6 regulates the neurogenetic gradient and neuronal identity in the thalamus. Proc. Natl. Acad. Sci. USA 106, 19895-19900.

Shinohara, K., Tominaga, K., Fukuhara, C., Otori, Y., and Inouye, S.I. (1993a). Processing of photic information within the intergeniculate leaflet of the lateral geniculate body: assessed by neuropeptide Y immunoreactivity in the suprachiasmatic nucleus of rats. Neuroscience 56, 813-822.

Shinohara, K., Tominaga, K., Isobe, Y., and Inouye, S.T. (1993b). Photic regulation of peptides located in the ventrolateral subdivision of the suprachiasmatic nucleus of the rat: daily variations of vasoactive intestinal polypeptide, gastrin-releasing peptide, and neuropeptide Y. J. Neurosci. 13, 793-800.

Szkudlarek, H.J., Herdzina, O., and Lewandowski, M.H. (2008). Ultra-slow oscillatory neuronal activity in the rat olivary pretectal nucleus: comparison



with oscillations within the intergeniculate leaflet. Eur. J. Neurosci. 27, 2657-2664

Thompson, S., Foster, R.G., Stone, E.M., Sheffield, V.C., and Mrosovsky, N. (2008). Classical and melanopsin photoreception in irradiance detection: negative masking of locomotor activity by light. Eur. J. Neurosci. 27, 1973-

Uchikawa, M., Kamachi, Y., and Kondoh, H. (1999). Two distinct subgroups of Group B Sox genes for transcriptional activators and repressors: their expression during embryonic organogenesis of the chicken. Mech. Dev. 84, 103-120.

van Eekelen, J.A., Bradley, C.K., Göthert, J.R., Robb, L., Elefanty, A.G., Begley, C.G., and Harvey, A.R. (2003). Expression pattern of the stem cell leukaemia gene in the CNS of the embryonic and adult mouse. Neuroscience 122, 421-436.

Viney, T.J., Balint, K., Hillier, D., Siegert, S., Boldogkoi, Z., Enquist, L.W., Meister, M., Cepko, C.L., and Roska, B. (2007). Local retinal circuits of melanopsin-containing ganglion cells identified by transsynaptic viral tracing. Curr. Biol. 17. 981-988.

Vue, T.Y., Aaker, J., Taniguchi, A., Kazemzadeh, C., Skidmore, J.M., Martin, D.M., Martin, J.F., Treier, M., and Nakagawa, Y. (2007). Characterization of progenitor domains in the developing mouse thalamus. J. Comp. Neurol. 505, 73-91.

Webb, I.C., Patton, D.F., Hamson, D.K., and Mistlberger, R.E. (2008). Neural correlates of arousal-induced circadian clock resetting: hypocretin/orexin and the intergeniculate leaflet. Eur. J. Neurosci. 27, 828-835.

Whiteley, S.J., Sauvé, Y., Avilés-Trigueros, M., Vidal-Sanz, M., and Lund, R.D. (1998). Extent and duration of recovered pupillary light reflex following retinal ganglion cell axon regeneration through peripheral nerve grafts directed to the pretectum in adult rats. Exp. Neurol. 154, 560-572.

Young, M.J., and Lund, R.D. (1994). The anatomical substrates subserving the pupillary light reflex in rats: origin of the consensual pupillary response. Neuroscience 62, 481-496.